Monte Carlo simulations and dynamic field theory for suspended particles in liquid crystalline systems

S. Grollau, E. B. Kim, O. Guzmán, N. L. Abbott, and J. J. de Pablo[a)]
Department of Chemical Engineering, University of Wisconsin—Madison, Madison, Wisconsin 53706

(Received 13 February 2003; accepted 23 April 2003)

Monte Carlo simulations and dynamic field theory are used to study spherical particles suspended in a nematic liquid crystal. Within these two approaches, we investigate the binding of the defects to the particles, the adsorption of a particle at a solid surface, and two particles interacting with each other. Quantitative comparisons indicate good agreement between the two approaches. A Monte Carlo method based on the combination of canonical expanded ensemble simulations with a density-of-state formalism is used to determine the potential of mean force between one particle and a hard wall. On the other hand, the potential of mean force is evaluated using a dynamic field theory, where the time-dependent evolution of the second rank tensor includes two major aspects of liquid crystalline materials, namely the excluded volume and the long-range order elasticity. The results indicate an effective repulsive force that acts between the particle and the wall. Layer formation at the surface of the hard wall gives rise to local minima in the potential of mean force. The director profile for a particle at contact with a solid surface is characterized by a disclination line distorted and attracted towards the wall. The structure of the nematic for two particles at short distances is also investigated. Our results indicate a structure where the two particles are separated by a circular disclination line. The potential of mean force associated with this configuration indicates an effective attractive interaction between the two particles. © *2003 American Institute of Physics.*
[DOI: 10.1063/1.1582843]

I. INTRODUCTION

Emulsions and colloidal suspensions are an abundant state of matter and have attracted considerable attention in condensed matter physics and technology. Systems consisting of colloidal particles suspended in a nematic liquid crystal exhibit distinctive features arising from the orientational order adopted by the liquid crystal molecules.[1] When the host fluid is a nematic, the anisotropic properties of the fluid can lead to anisotropic interactions between the suspended particles. The characteristics of the colloidal interactions depend on details of the system such as the strength of the anchoring or the orientation of the liquid crystal molecules at the colloidal particle surface. For sufficiently strong anchoring, spherical particles can create topological defects in the nematic phase. These defects appear at a well-defined distance from the particles. The resulting director configurations induce distortions of the uniform nematic order that are responsible for the occurrence of anisotropic forces.

Recent experiments have opened a new and promising area for application of liquid crystal-based devices.[2] These experiments show that liquid crystalline materials can be used for optical amplification of ligand–receptor binding, thereby providing the basis for design of biosensors. Optical amplification of binding events at a surface relies on the optical properties of a liquid crystal and its ability to form highly oriented phases. By using appropriate surface treatments, such as chemisorption of alkanethiols on gold surfaces,[3] a long-range, uniform orientation can be induced throughout a liquid crystal film on a substrate. Upon binding of proteins or viruses to that substrate, however, the long-range order can be destroyed through the occurrence of topological defects, giving rise to a clear optical signal that can be detected visually.

In the case of colloidal systems or emulsions, a so-called director description is often appropriate to investigate the structure of the nematic at micrometer length scales and around colloidal particles. However, in the design of optical biosensors, the characteristic sizes of the particles immersed in the nematic (proteins or viruses) are of order 10 to 100 nanometers. For submicron particles, description of the structure of the nematic in terms of the director (representing the average orientations of the molecules in the nematic phase) can be inappropriate. The investigation of the structure of a nematic around submicron particles requires either the introduction of more microscopic degrees of freedom than in a director description (in order to treat and describe the presence of topological defects[4]) or a molecular-level description.

In the case of perpendicular orientations of the molecules at the colloidal surface (strong homeotropic anchoring), colloids can create a satellite dipolar configuration (the so-called hedgehog defect) known to be more favorable for particles whose size is large compared to the nematic correlation length. For smaller particles, colloids can create a configuration with a ring disclination line around the particle (the so-called Saturn ring defect). Following the early work of Brochard and de Gennes in the one constant approximation,[5] the director distribution around colloidal

a)Electronic mail: depablo@engr.wisc.edu

particle has been considered in several theoretical studies based on a director description and ansatz functions.[6–8] In Ref. 7, the effects of strength anchoring on the director configuration are investigated using ansatz functions and by considering the linear regime of weak anchoring limit. The nonlinearity of the Euler–Lagrange equations that describe the elastic deformations of the nematic liquid crystal makes these problems nontrivial, and numerical simulations have become more common. For instance, the effects of strength anchoring have been investigated using Monte Carlo simulations within the director description,[9] and several authors have investigated the effects of the particle size, external field, and the presence confining surfaces through numerical minimization of the Frank free energy.[10,11] The configuration of nematogens around a spherical particle has also been studied with molecular dynamics simulations.[12,13]

In this work, two different approaches are used to examine the behavior of suspended particles in liquid crystalline systems: Monte Carlo simulations and dynamic field theory. A Monte Carlo method based on the combination of canonical expanded ensemble simulations and a density-of-states formalism is implemented to study the nature of liquid crystal mediated effective interactions. A dynamic field theory on the second rank tensor is developed and solved numerically. This approach permits study of the relaxation of the nematic, the dynamic behavior of defects, the equilibrium structure of the nematic, and the free energy of the system. With these two approaches, we investigate the structure of the nematic around particles of various sizes, effective potentials between a particle and a substrate, and also between two particles. This study provides an understanding of the interplay between director configurations and the nature of the colloidal interactions. In particular, we find that when two particles are at close distance, interactions between distinct defects yield new configurations and an effective attractive force. A quantitative mapping between the results of Monte Carlo simulations and field theory is presented to analyze the limits of validity of the theory.

The paper is organized as follows. In Sec. II we present the Monte Carlo method. In Sec. III we present the dynamic field theory on the second rank tensor. Our results are presented and analyzed in Sec. IV.

II. EXPANDED DENSITY-OF-STATES METHOD

The interaction between a colloidal particle and a hard wall (or also between two colloidal particles) can be quantified through a potential of mean force. The potential of mean force (PMF) provides a measure of the effective difference in the free energy between two states as a function of a specific degree of freedom of the system. This degree of freedom, referred to as reaction coordinate, can be a physical coordinate. In this work, the reaction coordinate ζ refers to the distance between a particle and a wall. The method used to evaluate the potential of mean force has been described recently.[14] It relies on a combination of a canonical expanded ensemble simulation with a density-of-states formalism.

The PMF is connected to the probability $p(\zeta)$ of finding the system of interest in a state, labeled by ζ, through the reversible work theorem[15]

$$w(\zeta) = -k_B T \ln p(\zeta), \tag{1}$$

where k_B is the Boltzmann constant and T is the temperature of the system. In Monte Carlo simulations, the probability of visiting high-energy states is low and their sampling is generally poor. To improve the sampling of these regions of phase space, it is often advantageous to constrain the reaction coordinate ζ or to introduce a biasing potential. Another way for sampling phase space more efficiently is through the use of expanded ensembles where intermediate states, not necessarily physical, are introduced to facilitate transitions between states separated by large energy barriers (see for instance Ref. 14 and references therein). The method used here consists of a combination of canonical expanded ensemble simulations with a density-of-states formalism.

The system is characterized by N mesogens in a volume V and at temperature T. We consider M subsystems along the reaction coordinate ζ such that the mth state corresponds to a given position of the colloidal particle specified by $\zeta = \zeta_m$. The values ζ_1, $\zeta_2 = \zeta_1 + \Delta\zeta, \ldots, \zeta_m = \zeta_1 + m\Delta\zeta, \ldots,$ and $\zeta_M = \zeta_1 + M\Delta\zeta$, define a "window" $[\zeta_1, \zeta_M]$ of the region of interest. The partition function Z of the expanded ensemble is given by

$$Z = \sum_{m=1}^{M} Z(N,V,T,m) g_m = \sum_{m=1}^{M} Z_m g_m, \tag{2}$$

where $Z_m(N,V,T,m)$ is a canonical partition function and g_m a positive weighting factor, both corresponding to the particular state m. The weighting factor g_m is determined self-consistently in a density-of-states formalism designed to provide uniform sampling of the states.

The probability p_m of finding the system in state m is given by

$$p_m = \frac{Z_m g_m}{Z}. \tag{3}$$

For any two states k and m

$$\frac{Z_m}{Z_k} = \frac{p_m g_k}{p_k g_k}, \tag{4}$$

and the difference in the free energy between two states m and k is given by

$$\Delta F = w(\zeta_m) - w(\zeta_k) = -\frac{1}{\beta} \ln \frac{Z_m}{Z_k}, \tag{5}$$

which, in terms of the weighting factors, can be written as

$$\Delta F = w(\zeta_m) - w(\zeta_k) = -\frac{1}{\beta}\{\ln p_m - \ln p_k - \ln g_m + \ln g_k\}. \tag{6}$$

(In what follows, ΔF denotes a difference between two potentials of mean force, determined from Monte Carlo simulations or from the field theory.) The interpretation of the weighting factors is apparent from Eq. (6): if the states are sampled uniformly during the simulations, such that p_k

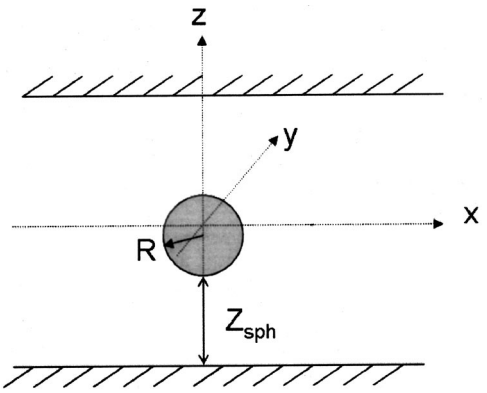

FIG. 1. Scheme of the system.

$=p_m$ for every state, the difference $\beta\Delta F$ is provided by $-\ln(g_k/g_m)$. Knowledge of g_m provides the density of the state m.

To achieve uniform sampling and evaluate g_m, a random walk is performed in the state m. During the course of the simulation, the colloidal particle and the mesogens are rearranged through arbitrary Monte Carlo moves. To study the interaction between a colloidal particle and a wall, we consider displacements $\Delta\zeta$ of the particle along the z axis, the walls being the horizontal top and bottom planes (see Fig. 1). Periodic boundary conditions are imposed in the other directions. The Monte Carlo moves for the mesogens consist of trial random rotations and displacements. Standard Metropolis criteria are implemented. A Monte Carlo cycle consists of a trial move of all liquid crystal molecules. After one cycle, a move from one state m to a new state k is attempted (displacement of a colloidal particle). The acceptance criteria for a trial move from an old to a new state are given by

$$P_{\mathrm{acc}}(\mathrm{old}\rightarrow\mathrm{new})=\min\{1,e^{-\beta(U_{\mathrm{new}}-U_{\mathrm{old}})-(\ln g_{\mathrm{new}}-\ln g_{\mathrm{old}})}\}$$
$$=\min\{1,e^{-\beta\Delta U-\Delta\ln g}\}. \tag{7}$$

Each time a new state is visited, the corresponding weighting factor g_{new} is modified by a convergence factor f greater than 1

$$g_{\mathrm{new}}\rightarrow f\cdot g_{\mathrm{new}}, \tag{8}$$

and the histograms of the corresponding state is updated. At the beginning of the simulation, the weighting factors g_m are set to be uniform. If the original state has a higher energy than the trial state, then the trial state can be easily visited, and g_{new} is updated. As the sampling of phase space proceeds during the simulation, the more often a state is visited the greater its weighting factor becomes. The ratio $g_{\mathrm{new}}/g_{\mathrm{old}}$ can eventually become smaller than unity. The system is therefore induced to sample states of phase space that have been less visited, promoting the sampling of high-energy states. Once a global histogram is sufficiently flat (the minimum population is enforced to be at least 85% of the average), a density-of-states Monte Carlo cycle is assumed to be completed. After that cycle, the convergence factor is altered by the square root function (any monotonically decreasing function with unity as the fixed point can be used) and a new Monte Carlo cycle is repeated. The cycles are performed until the running estimate of the weighting factors converge to the density of states. (The threshold value is fixed at $\ln f<0.006\,25$).

Simulations were performed with a system containing 11 460 liquid crystal molecules and were conducted with the same parameters as in Ref. 14. Namely, mesogens interact via a shifted and truncated repulsive Gay–Berne (GB) potential[16]

$$U_{ij}=4\epsilon_0(\varrho_{ij}^{-12}-\varrho_{ij}^{-6})+\epsilon_0,\quad \varrho_{ij}^{6}<2 \tag{9}$$
$$=0,\quad \varrho_{ij}^{6}>2, \tag{10}$$

with

$$\varrho_{ij}=(|\mathbf{r}_{ij}|-\sigma_{ij}+\sigma_0)/\sigma_0, \tag{11}$$

$$\varrho_{ij}=\sigma_0\left[1-\frac{\chi}{2}\left\{\frac{(\hat{\mathbf{r}}_{ij}\cdot\hat{\mathbf{u}}_i+\hat{\mathbf{r}}_{ij}\cdot\hat{\mathbf{u}}_j)^2}{1+\chi\hat{\mathbf{u}}_i\cdot\hat{\mathbf{u}}_j}+\frac{(\hat{\mathbf{r}}_{ij}\cdot\hat{\mathbf{u}}_i+\hat{\mathbf{r}}_{ij}\cdot\hat{\mathbf{u}}_j)^2}{1-\chi\hat{\mathbf{u}}_i\cdot\hat{\mathbf{u}}_j}\right\}\right]^{-1/2}, \tag{12}$$

and

$$\chi=\frac{\kappa^2-1}{\kappa^2+1}, \tag{13}$$

where $\hat{\mathbf{u}}_i$ denotes the molecular orientation along the main axis of the ellipsoid i, $\mathbf{r}_{ij}$ denotes the intermolecular vector $\mathbf{r}_{ij}=\mathbf{r}_i-\mathbf{r}_j$, with $\mathbf{r}_i$ the position of the mesogen i. (Unit vectors are identified with hats, $\hat{\mathbf{r}}_{ij}=\mathbf{r}_{ij}/|\mathbf{r}_{ij}|$; σ_0 corresponds to the width of the ellipsoids, and their length-to-width ratio is fixed at $\kappa=3$). The interactions of mesogens with the surface of the sphere and with the walls are described also by a shifted Gay–Berne potential defined, respectively, by

$$\varrho_{\mathrm{isph}}=(|\mathbf{r}_i-\mathbf{r}_{\mathrm{sph}}|-R+\sigma_0/2)/\sigma_0, \tag{14}$$

and

$$\varrho_{\mathrm{iwall}}=(|z_i|-z_{\mathrm{wall}}+\sigma_0/2)/\sigma_0. \tag{15}$$

Two walls, located at $z=\pm z_{\mathrm{wall}}$, are separated by a distance equal to $34\sigma_0$; $\mathbf{r}_{\mathrm{sph}}$ and $|z_i|-z_{\mathrm{wall}}$ denote, respectively, the position vector for the center of mass of the sphere and the normal distance between mesogen i and a wall. The radius of the sphere is denoted by R. In what follows, z_{sph} is the normal distance between the surface of the colloidal particle and the wall. This definition of z_{sph} is adopted both in Monte Carlo simulations and dynamic field theory (see Fig. 1 for an illustration of the system and the notations). The reduced density $\rho^*=\rho\sigma_0^3$ of the system is fixed at $\rho^*=0.335$ and simulations are conducted at constant temperature $T^*=k_BT/\epsilon_0=1$. The estimation of the weighting factors is performed on several overlapping windows $[\zeta_1,\zeta_M]$ for the physical coordinate $\zeta=z_{\mathrm{sph}}$. Each overlapping window $[z_{\mathrm{sph}}^1,z_{\mathrm{sph}}^M]$ consists of 200 states with $\Delta z=0.01$. The PMF between a colloidal particle and a hard wall is determined with simulations over nine windows. Initially, all weighting factors g_m and the convergence factor are set equal to $e^{0.1}$. To generate director configurations or density profiles, the coordinate ζ is fixed and standard Monte Carlo simulations are performed.

III. DYNAMIC FIELD THEORY

The second approach is a based on a dynamic field theory for the second rank tensor. At the microscopic level, nematogens are characterized by a nonisotropic distribution function $\psi(\hat{\mathbf{u}})$, which measures the probability that a molecule is oriented in the $\hat{\mathbf{u}}$ direction. A quantity that captures the anisotropy of the fluid is the symmetric traceless tensor order parameter

$$\mathbf{Q}_{ij}=\langle u_i u_j-\tfrac{1}{3}\delta_{ij}\rangle, \tag{16}$$

where the brackets $\langle A\rangle=\int A\psi(\hat{\mathbf{u}})d\hat{\mathbf{u}}_s$ denote an average over all possible orientations on the unit sphere. In the present description, the tensor order parameter $\mathbf{Q}(\mathbf{r})$ defines a coarse-grained order parameter that represents the local average Eq. (16) at point $\mathbf{r}$. (In what follows, the usual sum over repeated indices is assumed.)

In the present model, the equilibrium properties of the liquid crystal are described by a Landau–de Gennes free energy[17] that comprises a contribution describing the long-range elastic forces dominant in the nematic phase

$$\mathcal{F}_e=\int d\mathbf{r}\,\frac{L_1}{2}(\partial_i Q_{jk})(\partial_i Q_{jk}), \tag{17}$$

where L_1 is a material-specific elastic constant, and a short-range elastic contribution of the form

$$\mathcal{F}_s=\int d\mathbf{r}\left\{\frac{A}{2}\left(1-\frac{U}{3}\right)Q_{ij}Q_{ij} -\frac{AU}{3}Q_{ij}Q_{ik}Q_{kj}+\frac{AU}{4}(Q_{ij}Q_{ij})^2\right\}. \tag{18}$$

Equation (18) describes the excluded volume effects responsible for the first-order transition from the isotropic to the nematic phase. In this model, the first-order transition occurs at a magnitude of the nematic potential $U=2.7$. (An interpretation of the phenomenological parameters A and U can be obtained from the description of the nematic with a kinetic theory for rod-like molecules.[18] The dimensionless nematic potential U can be related to the number of molecules per unit of volume; the coefficient A has dimensions of pressure and represents in essence nk_BT, where n is the number density of rod-like molecules.) The strength of the two contributions, Eq. (17) and Eq. (18), depends on the liquid crystal of interest. For polymeric liquid crystals, short-range interactions are expected to be dominant, whereas long-range interactions are dominant for low-molecular weight liquid crystals. Parameter A permits control of the relative magnitude of the two contributions. For given values of the phenomenological parameters that arise in this theory, it is convenient to introduce the quantity $\xi=\sqrt{18L_1/AU}$ as a characteristic length scale for changes of the order parameter.

The time evolution equation for $\mathbf{Q}$ is obtained from the molecular field $\mathbf{H}$ that provides the driving force responsible for the relaxation of the order parameter towards the minimum of the free energy

$$\frac{\partial\mathbf{Q}}{\partial t}=\Gamma\mathbf{H}. \tag{19}$$

The molecular field is given by

$$\mathbf{H}=-\frac{\delta\mathcal{F}}{\delta\mathbf{Q}}+\frac{\mathbf{I}}{3}\,\mathrm{Tr}\,\frac{\delta\mathcal{F}}{\delta\mathbf{Q}}, \tag{20}$$

where $\mathcal{F}=\mathcal{F}_s+\mathcal{F}_e$ is the total free energy, $\mathbf{I}$ is the identity operator, and the last term arises from the minimization of the free energy keeping the order parameter $\mathbf{Q}$ traceless. From Eqs. (17)–(20), and by identifying the coefficient Γ with the rotational diffusivity coefficient D^* through the relation $\Gamma=6D^*/(1-\frac{3}{2}Q_{mn}Q_{mn})^2$, one obtains the following equation of motion for the components of the tensor order parameter:

$$\frac{\partial Q_{ij}}{\partial t}=-\frac{6D^*}{\left(1-\frac{3}{2}Q_{mn}Q_{mn}\right)^2}\left\{A\left(1-\frac{U}{3}\right)Q_{ij} -AU\left(Q_{im}Q_{mj}-\frac{\delta_{ij}}{3}Q_{mn}Q_{mn}\right) +AUQ_{ij}(Q_{mn}Q_{mn})-L_1\partial_\rho\partial_\rho Q_{ij}\right\}. \tag{21}$$

The above equation gives the time-evolution equation for the order parameter and represents a particular case of the Beris–Edwards formulation.[19] An important property of the time-evolution equation (Eq. (21) is that it is not restricted to the neighborhood of the first-order phase transition, but it also extends into the nematic phase for high values of the nematic potential U.

In the most general situation, the diagonalization of the tensor order parameter has the form

$$\mathbf{Q}=\begin{pmatrix}\frac{2S}{3} & 0 & 0\\ 0 & \frac{\eta-S}{3} & 0\\ 0 & 0 & -\frac{\eta+S}{3}\end{pmatrix}, \tag{22}$$

where S denotes the nematic scalar order parameter and η denotes the biaxiality. The eigenvector associated with the highest eigenvalue $2S/3$ corresponds to the generalization of the director $\mathbf{n}$.

At bounding surfaces, we assume that $\mathbf{Q}$ is uniaxial and has the form

$$\mathbf{Q}=S^{\mathrm{eq}}(\mathbf{nn}-\tfrac{1}{3}\mathbf{I}), \tag{23}$$

where $\mathbf{n}$ is the director at the surface, and S_{eq} is the equilibrium nematic order parameter given in the Doi theory[18] by

$$S^{\mathrm{eq}}=\frac{1}{4}+\frac{3}{4}\sqrt{1-\frac{8}{3U}}. \tag{24}$$

In the unaxial limit, the material specific elastic constant L_1 is related to the splay K_{11}, bend K_{22}, and twist K_{33} constants, through the relations[19] $L_1=K_{11}/S^2=K_{22}/S^2=K_{33}/S^2$, which correspond to the one-constant approximation.

The calculations are performed with a set of parameters that is representative of a low molecular weight liquid crystal such as pentylcyanobiphenyl (5CB) (see Ref. 20 for the simulation parameters). The nematic potential U can be chosen to give the same equilibrium value S^{eq} as observed in the Monte Carlo simulations. To compare results from theory and Monte Carlo simulations, U is fixed at $U=4.8$, which leads to the equilibrium value $S_{eq}=0.75$. This equilibrium value corresponds to that observed in Monte Carlo simulations when the bulk density is fixed at $\rho^*=0.335$. The system is the same as in Monte Carlo simulations and corresponds to a particle confined between two walls (see Fig. 1). We consider the case of strong homeotropic anchoring (molecules oriented perpendicularly to the surface) at the surface of the particle and at the surface of the walls. Periodic boundary conditions are imposed in the other directions. All calculations are performed with an initial configuration that corresponds to a uniform nematic order where all molecules point in the z direction. The director is initially aligned along the z direction with $\mathbf{n}=(0,0,1)$ and the nematic scalar order parameter is fixed at the equilibrium value Eq. (24). The corresponding initial tensor $\mathbf{Q}$ in the simulation box is uniaxial and given by Eq. (23). The relaxation of the nematic is obtained by numerical integration of Eqs. (21). A Euler scheme is used to solve these equations. Derivatives are evaluated by finite difference methods on a regular grid. The insertion of a particle is implemented automatically in the numerical procedure, where the grid is defined in the entire area of interest except in the region inside the particle. Two- and three-dimensional simulations are performed in this work. We have used different mesh divisions for the spatial resolution of the grid and also several time steps to verify the stability of the numerical resolution (see Ref. 21 for the grid parameters). The resolution is performed on the six components of $\mathbf{Q}$, which allows us to verify that the traceless condition, $Q_{xx}+Q_{yy}+Q_{zz}=0$, is satisfied at each time step.

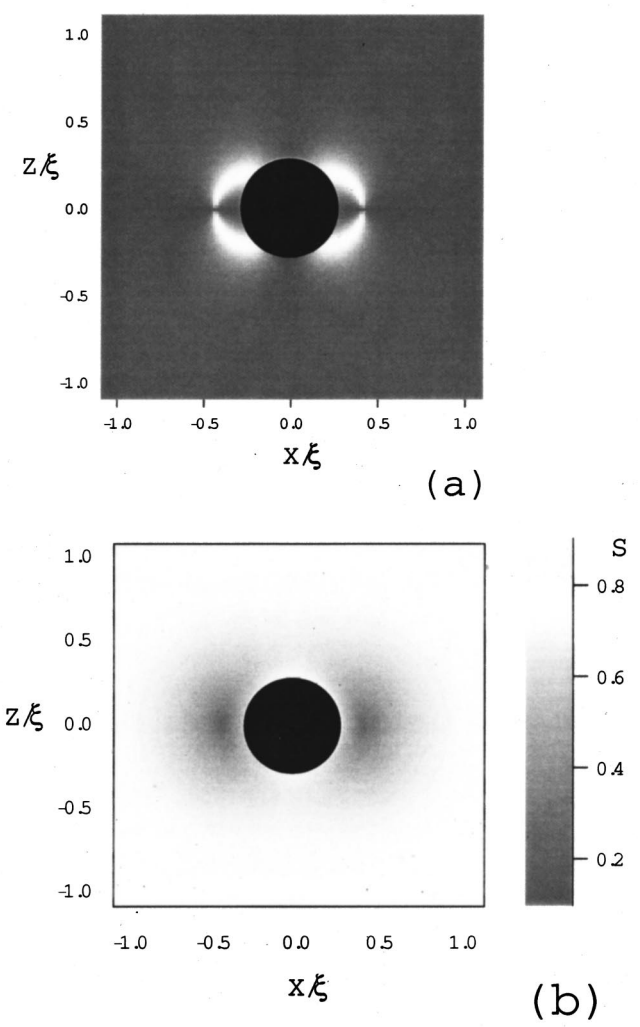

FIG. 2. Particle in uniform nematic: optical picture for the director profile (a) and nematic scalar order parameter S (b), from the theory (2D system).

IV. RESULTS AND DISCUSSION

A. One particle in a nematic liquid crystal: Binding of topological defects and deviations from the director description

We first consider the insertion of one spherical particle into a nematic liquid crystal. The particle is fixed in the middle of the cell (both in simulations and in the theory).

Simulations and theory indicate that the particle is surrounded by a Saturn ring disclination line. Figure 2 shows the director profile and the order parameter at equilibrium. For the director profile, the ''optical'' picture is obtained by assigning a color proportional to $(n_x n_z)^2$, and representative of the intensity of light transmitted through two crossed polarizers in the x- and z directions. In this optical picture, the Saturn ring ($-1/2$ disclination line) is characterized by two bright brushes in the equatorial plane of the particle. For the nematic scalar order parameter map, a color is attributed to S depending on its magnitude (dark colors for low values of S). The results from the theory are obtained from two-dimensional calculations. During the relaxation of the liquid crystal, the defects are first created in the neighborhood of the particle; they are then repelled from the surface of the particle until they reach an equilibrium position. (We have observed that in three dimensions, the particle is also surrounded by a Saturn ring. See Ref. 22 for details.) Figure 3 reports the director profile obtained from Monte Carlo simulations for a particle of radius $R=4\sigma_0$. The director profile is also characterized by a Saturn ring defect located in the equatorial plane of the particle.

Two configurations are possible for homeotropic anchoring at the surface of the particle: a Saturn ring or a hedgehog configuration. The Saturn ring configuration obtained in this work is due to the fact that the particles considered here are relatively small. In Monte Carlo simulations, the radius of the particle is of the order of several molecular lengths σ_0. In the theory, the radius of the particle is of order ξ, the characteristic length for changes of the order parameter. For such particle sizes, the Saturn ring configuration is expected to be more stable than the hedgehog configuration. This is also suggested by previous numerical analyses on the stability of the defects showing that a Saturn ring configuration is stable for particles with radii smaller than $R\approx 250$ nm.[10,11]

We have analyzed the location of the ring defect a, with

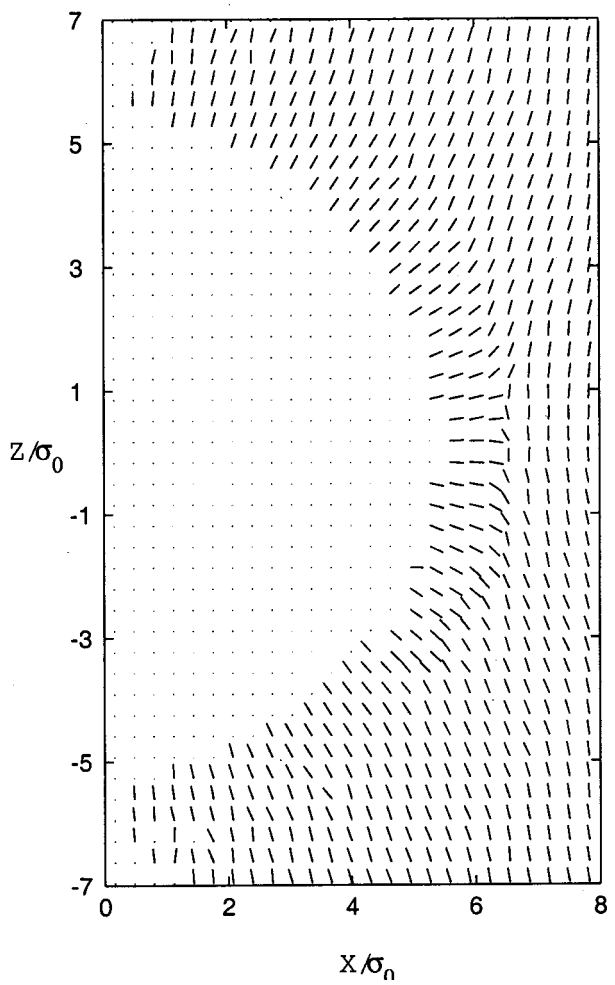

FIG. 3. Particle in uniform nematic: director profile, from Monte Carlo simulations.

both approaches, for various radii R of the particle. At the point defect the scalar order parameter exhibits a minimum (see Fig. 2). The location of the defect is determined by looking for the minimum value in the scalar order parameter S. The results are reported in Figs. 4 and 5, for the theory and for the Monte Carlo simulations, respectively. For the theoretical results, lengths are given in units of ξ; for Monte Carlo results, lengths are given in units of σ_0. From Fig. 4, one observes that as the size of the particle increases, the defect is bound to the particle at a distance a that is a linear function of the radius, with $a \approx 1.20R$ (see the data for $R = 2.7\xi$ and $R = 4.4\xi$). As indicated by Fig. 5, Monte Carlo simulations suggest that for a large particle, the ratio a/R tends to a constant value of approximately 1.2. This value obtained for a large particle is consistent with that obtained within the framework of the continuum theory (or equivalently with the director description). Indeed, previous analyses based on the numerical minimization of the Frank free energy give $a \approx 1.10R$ for the location of the defect.[10,11] In these studies, the difference in the elastic constants is probably responsible for the quantitative difference in the ratio a/R. Previous estimates (made in the one constant approximation) give $a \approx 1.22R$ from Monte Carlo simulations,[9] and $a = (7/3)^{1/4}R \approx 1.236R$ within the electrostatic analogy.[23]

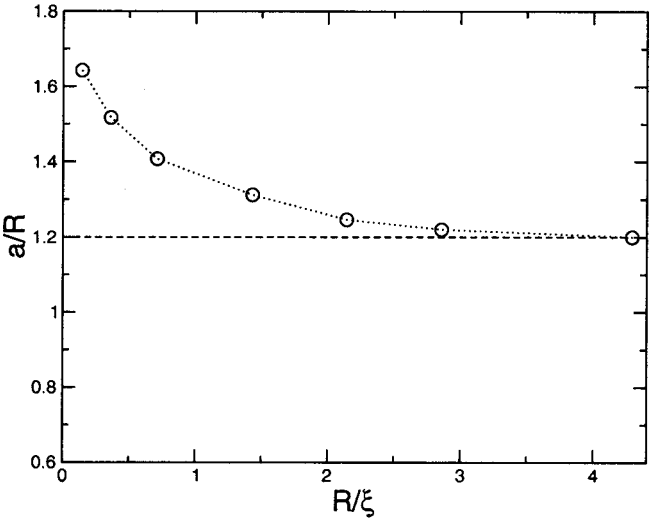

FIG. 4. Location of the defect a/R for various particle radii R, from the theory. The dashed line represents $a/R = 1.20$.

These values are similar to the one observed here in the limit of large particles.

As the size of the particle decreases, results from Figs. 4 and 5 show deviations from the linear behavior. In the limit of large particles, the spatial extension of the core defect can be neglected. The description of the structure of the nematic in terms of the director is thus appropriate, and leads to a constant ratio a/R. However, for submicron particles, the linear regime is no longer valid, emphasizing the fact that the spatial extension of the defect cannot be neglected. Our results indicate that departures from the continuum theory appear for particle radii smaller than $R \approx 8\sigma_0$ in Monte Carlo simulations, and for radii smaller than $R \approx 4\xi$ in the theory. This analysis provides a basis to establish a correspondence between the width of the mesogens σ_0 (in the molecular description) and the characteristic length ξ of the theory, $\xi \sim 2\sigma_0$. Using the correspondence $\xi = 2\sigma_0$, the results obtained from the theory for the location of the defects are

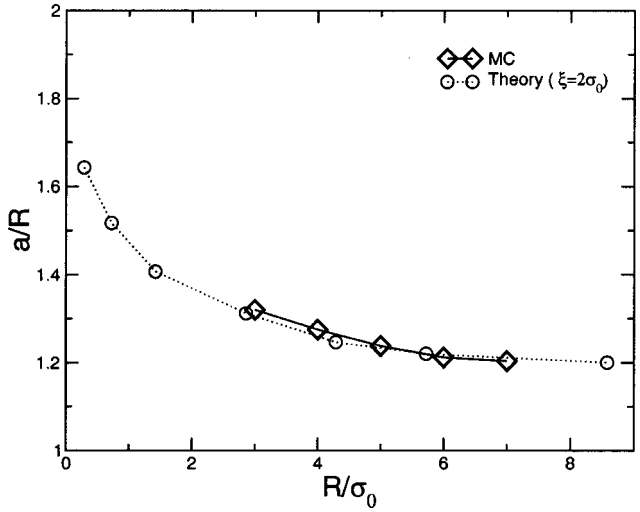

FIG. 5. Location of the defect a/R for various particle radii R, from Monte Carlo simulations (diamonds). Results from the theory (circles) have been reported using the correspondence $\xi = 2\sigma_0$.

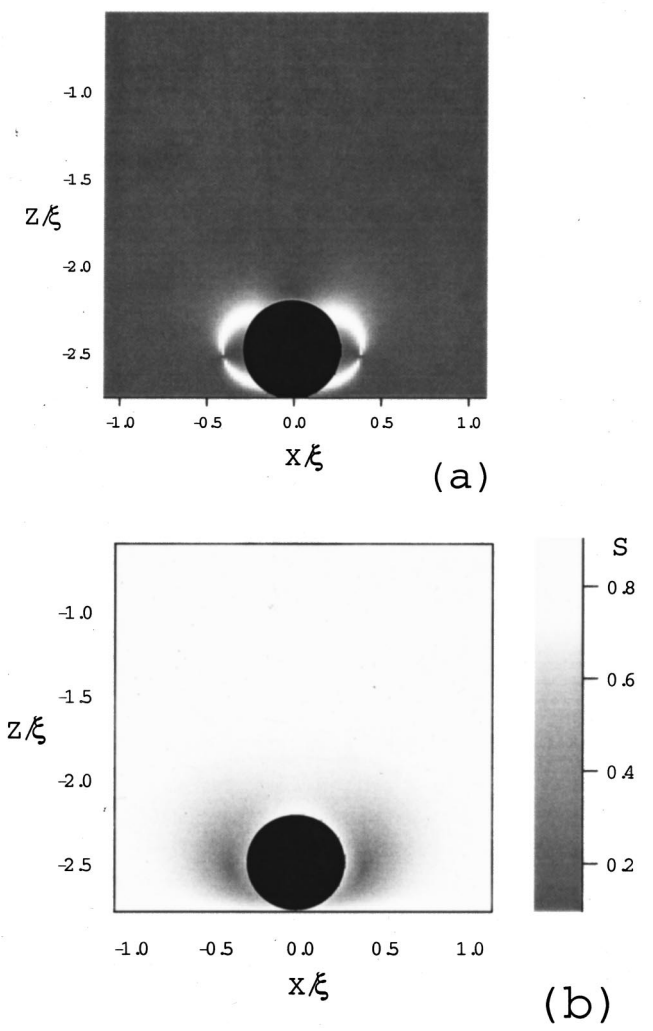

FIG. 6. Particle at contact with a solid surface: optical picture (a), nematic scalar order parameter S (b), from the theory (2D system).

reported in Fig. 5, where the lengths have been scaled in units of σ_0 in order to make the comparison with Monte Carlo results. This first comparison between theory and simulations shows good agreement, suggesting that the molecular model is well represented by the present dynamic theory.

B. Interaction between a particle and a wall

In this section we consider the interaction between a particle and a wall. We first present the results from theory. Figure 6 shows the optical picture giving the director profile and the nematic scalar order parameter for a two-dimensional system. A particle of radius $R=0.36\xi$ is located at the surface of the wall. The comparison between this figure and the structure obtained for a particle in the middle of the cell (see Fig. 2) indicates that the defects are no longer in the equatorial plane, but are shifted towards the wall. This is revealed by the optical picture and also by the position of the minimum in the order parameter. Similar deviations for the location of the rings are observed from Monte Carlo simulations. Figure 7 shows the dimensionless potential of mean force, ΔF, obtained from the theory as a function of the separation

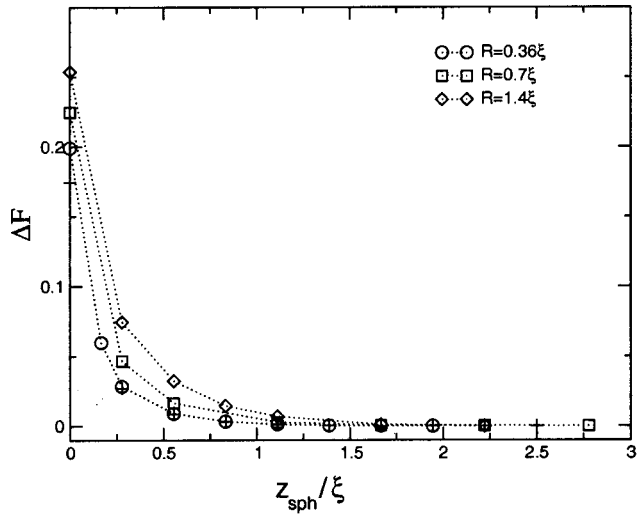

FIG. 7. Potential of mean force between a particle and a solid surface, from the theory (2D system).

z_{sph} between the particle and the wall. (In what follows, ΔF is defined as the free-energy difference between a given position of the particle with the particle located in the middle of the cell.) The potential of mean force ΔF is reported for three different radii of the particle, namely $R=0.36\xi$, $R=0.7\xi$, and $R=1.4\xi$. Figure 8 shows the potential of mean force obtained from Monte Carlo simulations. Simulations are performed for particle radii, $R=3\sigma_0$, $R=4\sigma_0$, $R=5\sigma_0$, and $R=6\sigma_0$. The theory predicts an increasing free-energy variation as the distance between the wall and the colloidal particle decreases; Monte Carlo simulations predict a global repulsive force, with the occurrence of oscillations and local minima. The occurrence of these local minima is due to the formation of smectic layers at the wall. Figure 9 shows a density map for the whole simulation cell for a particle of radius $R=3\sigma_0$ fixed at the surface of the wall.

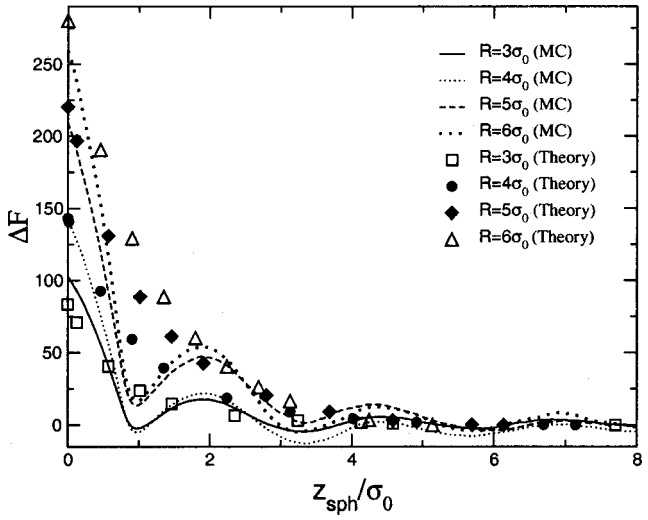

FIG. 8. Potential of mean force between a particle and a solid surface, from Monte Carlo simulations (curves). The symbols correspond to potential of mean force estimates obtained from the theory (3D system). Theoretical results are scaled using the correspondence $\xi\approx 2\sigma_0$ and one single factor for the free-energy units (see the text).

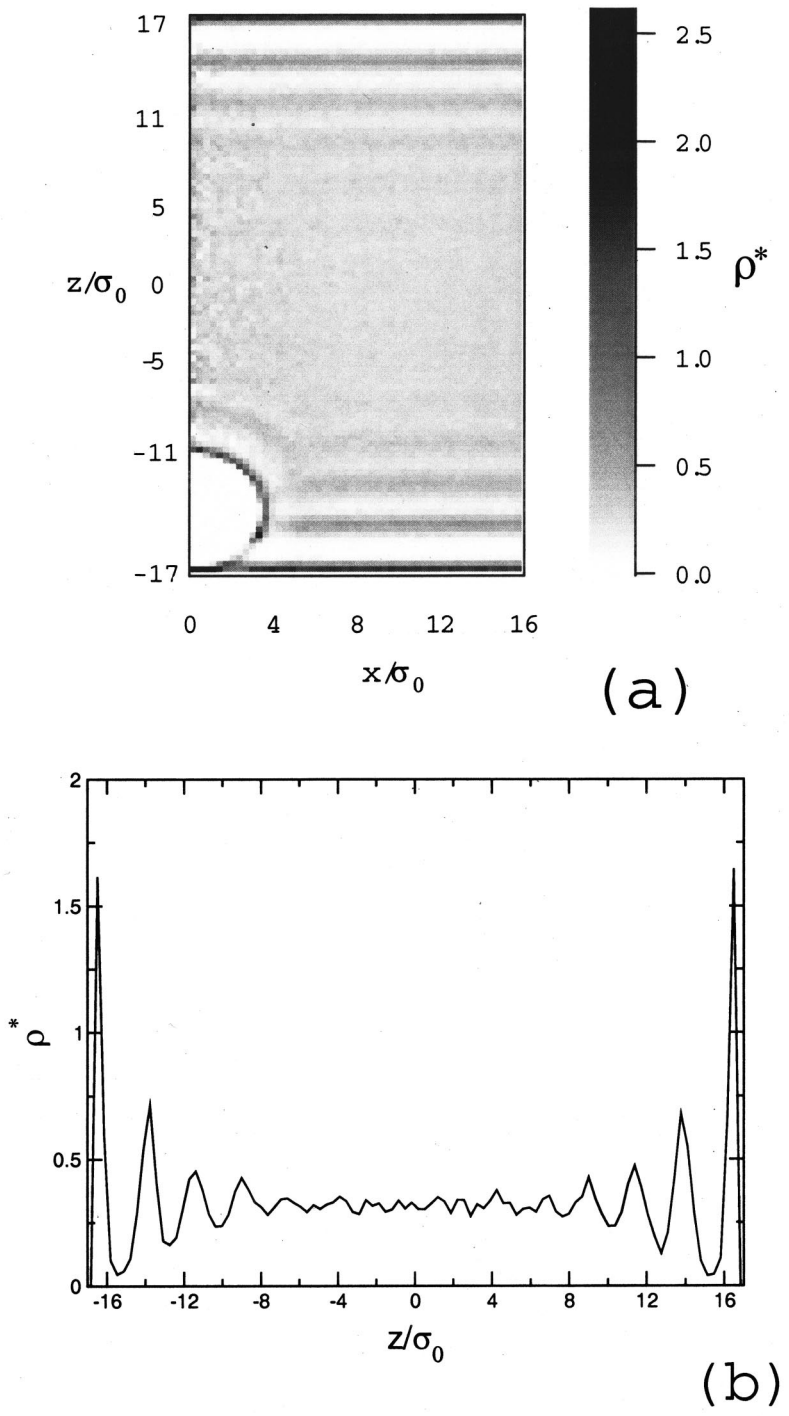

FIG. 9. Density map (a) and density profile across the cell at $x/\sigma_0=10$ (b). (The radius of the particle is $R=3\sigma_0$.)

The color is proportional to the average density, with dark colors for high density. The density curve in Fig. 9 gives the density profile across the cell and between the two walls at position $x=10\sigma_0$. From the density profile, it can be seen that, near the walls, liquid crystal molecules are densely packed and form several layers. The presence of these layers is responsible for the metastable positions of the particle; configurations with the particle trapped between two layers are more stable. These features, which originate in the molecular structure of the system, cannot be captured by the dynamic field (which yields a monotonic potential of mean force). It is interesting to compare quantitatively the two approaches. For that purpose, calculations have been performed in three dimensions with the theory, for four particles of radius $R=1.5\xi$, $R=2.0\xi$, $R=2.5\xi$, and $R=3.0\xi$ (according to our previous mapping $\xi=2\sigma_0$, these radii correspond to $R=3\sigma_0$, $R=4\sigma_0$, $R=5\sigma_0$, and $R=6\sigma_0$, respectively). The corresponding potentials of mean force as the particles approach the walls are reported in Fig. 8. The free-energy estimates provided by the theory and Monte Carlo simulations are given in different units; a correspondence between the two approaches is established as follows. We rescale the free-energy units obtained from the theory using a single multiplicative factor. This factor is determined by matching

the maximum $\Delta F_{\max}(z_{\mathrm{sph}}=0)$ obtained from the simulations for $R=4\sigma_0$, with the maximum $\Delta F_{\max}(z_{\mathrm{sph}}=0)$ obtained from the theory for $R=4\sigma_0$. The same factor is used to rescale the potential of mean force for the other particle radii. Figure 8 shows that the agreement between the two approaches is quantitative: the results obtained from the theory basically constitute a smooth average of the free-energy curves obtained from the simulations. The particle size effect and the range of repulsion are captured quantitatively by the theory down to molecular length scales.

We conclude this section with the following comment on the comparison between the two approaches. Experimentally, the orientations of the liquid crystal molecules and the strength of the anchoring at the various surfaces depend on the system under study. For instance, in emulsions, the anchoring properties can be controlled using various amphiphilic compounds adsorbed at the droplet–liquid crystal interface.[24] In the case of solid surfaces, the anchoring properties can be controlled using self-assembled monolayers of different compositions.[3] Past studies on the effect of anchoring strength show that the distance between the defects and the colloidal surface,[9] as well as the nature of the interaction between a particle and a solid surface,[25] depend on the anchoring properties of the system. In this work we have only considered the case of strong homeotropic anchoring in the theoretical description. In the molecular description, the anchoring properties result from the choice of the potential. The potential used here is the same as that employed in a previous study of a colloidal particle in a bulk liquid crystal.[13] This choice of potential gives rise to strong homeotropic anchoring properties (molecules oriented perpendicularly to the surface). The very good quantitative agreement observed between theory and simulations for both the location of the defects (of different particle radii) and the interaction between a particle and solid surface indicate that the dynamic theory employed here gives a good description of the molecular description when molecules exhibit strong homeotropic anchoring properties at the various surfaces in the system. In that limit, the theory can be used to investigate the structure of the nematic around small particles, down to molecular length scales, with the caveat that the density profile and layer formation cannot be captured by the theory.

C. Two particles in a nematic liquid crystal at short distance

In this section, we use the theory to study the interaction between two particles at short distances in a uniform nematic liquid crystal.

For particles surrounded by Saturn ring defects, previous calculations of the long-range pair potential within the director description[26] indicate that the nature of the colloidal interaction depends on the particles' position with respect to the direction of the uniform nematic order. This study[26] indicates a long-range repulsive force when the two particles are aligned along the direction of uniform nematic order, and also when particles are located in the plane perpendicular to this direction. An attractive force between the two particles occurs at a certain oblique angle. Here, we investigate the structure of the nematic and the nature of colloidal interactions when the particles are at short distances, and we restrict our analysis to the case where particles are located in a plane perpendicular to the direction of the nematic order (particles at the same z coordinate with a uniform nematic order in the z direction).

We first consider the case of two particles in two dimensions. Figure 10 shows optical pictures of the equilibrium configurations for particles of radii $R=3.3\xi$ at the three distances $d_{\mathrm{surf}}=1.1\xi$, $d_{\mathrm{surf}}=3.3\xi$, and $d_{\mathrm{surf}}=6.1\xi$, where d_{surf} denotes the distance between the two colloidal surfaces. At large distances ($d_{\mathrm{surf}}=6.1\xi$), the equilibrium configuration is characterized by particles surrounded by two Saturn rings. For particles at short distances, we observe that the defects that are first created at the surface of the particles can interact with each other during relaxation, leading to different structures; see Fig. 10 for $d_{\mathrm{surf}}=1.1\xi$ and $d_{\mathrm{surf}}=3.3\xi$. In that case, equilibrium configurations are characterized by two topological defects located in the midplane separating the two particles. As the distance between the two particles increases, the two topological defects in the midplane approach each other (see the optical picture for $d_{\mathrm{surf}}=3.3\xi$). Figure 11 reports the potential of mean force as a function of the distance d_{surf}. Calculations are presented for particle radii $R=2.8\xi$, $R=3.3\xi$, and $R=3.9\xi$. From these results, one can observe that the colloidal interaction is characterized by three regions: a repulsive force at contact and for $d_{\mathrm{surf}}/\xi\leqslant 1$, an effective attractive force for distances in the range $1\leqslant d_{\mathrm{surf}}/\xi\leqslant 5$, and a repulsive force at longer distances $d_{\mathrm{surf}}/\xi\geqslant 5$. The repulsion at contact is explained by the anchoring properties at the particles' surface. The strong homeotropic anchoring properties at the circular surfaces induce an increase in the free energy when particles are at contact. This repulsion is similar to that observed for a particle interacting with a solid surface, with a characteristic range of order ξ (see Figs. 7 and 8, which also suggest a characteristic interaction range of order ξ). When the distance between the two particles increases in the range $1\leqslant d_{\mathrm{surf}}/\xi\leqslant 5$, the effective force becomes attractive. This attraction corresponds to a ''binding'' between the two particles created by the two defects located in the midplane (see Fig. 10). For the particles considered here, the range of the attractive force is found to be of order 5ξ. At longer distances $d_{\mathrm{surf}}\geqslant 5\xi$, one observes a slow decay of ΔF and a repulsive force. For long distances between the particles, $d_{\mathrm{surf}}\geqslant 5\xi$, the director configuration as shown in Fig. 10 is that of two particles surrounded by their own Saturn rings. In that case, the potential of mean force shows a repulsive force between the particles. The occurrence of the repulsive force for particles surrounded by its Saturn ring is in qualitative agreement with the results of a literature study.[26] In that work, the pair interaction potential between two macroscopic particles surrounded by a Saturn ring was determined from the linear regime of weak anchoring limit; in that limit a repulsive force is observed at long distances when particles are oriented perpendicular to the direction of the nematic order. In the present work, we consider the interaction between particles that are small (several molecular lengths). As indicated

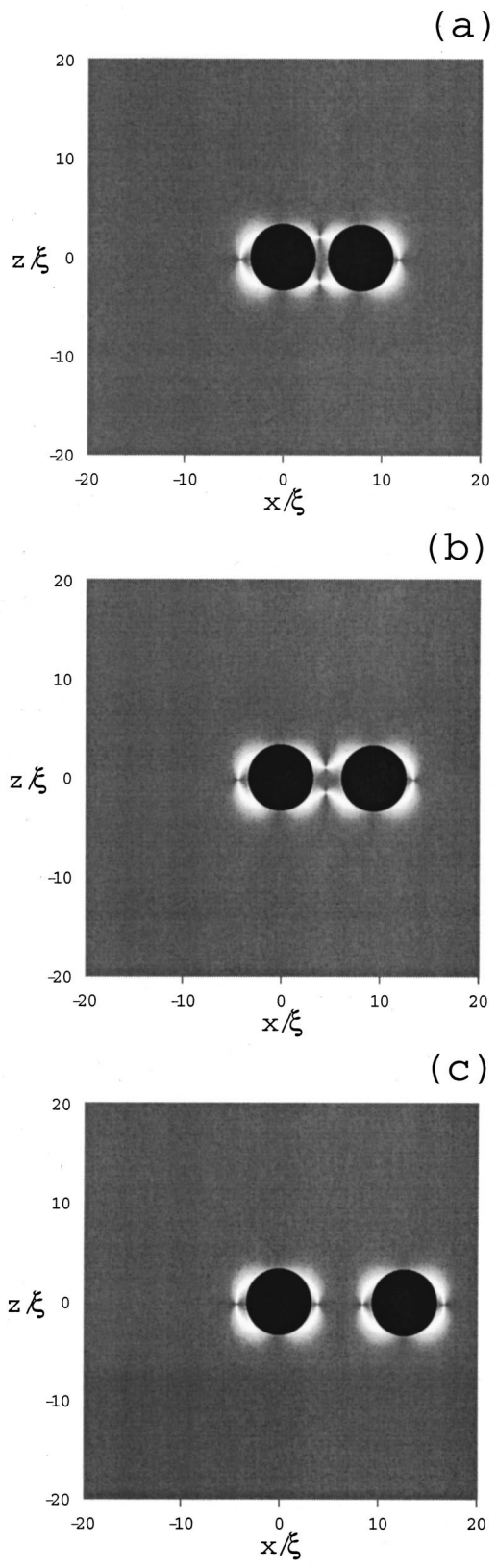

FIG. 10. Director profile for two particles of radius $R=3.3\xi$. Optical picture for distances between the colloidal surfaces, $d_{surf}=1.1\xi$ (a), $d_{surf}=3.3\xi$ (b), and $d_{surf}=6.1\xi$ (c), from the theory (2D system).

by Fig. 11, for such small particles, the repulsive force is present but it vanishes rapidly, as shown by a potential of mean force that tends to a constant value for $d_{surf}/\xi \geqslant 8$.

The structure of the nematic, revealed by our calcula-

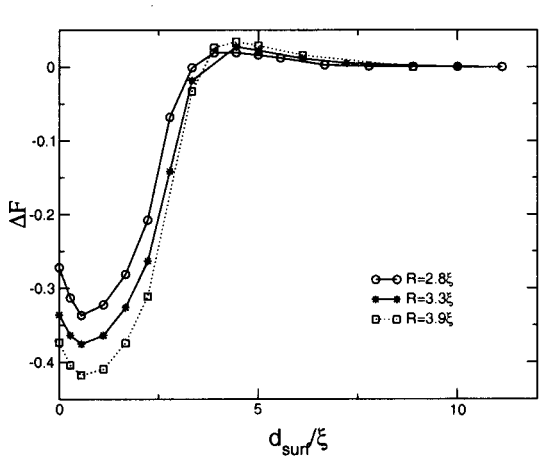

FIG. 11. Potential of mean force ΔF as a function of the distance between the two colloidal surfaces d_{surf}, from the theory (2D system).

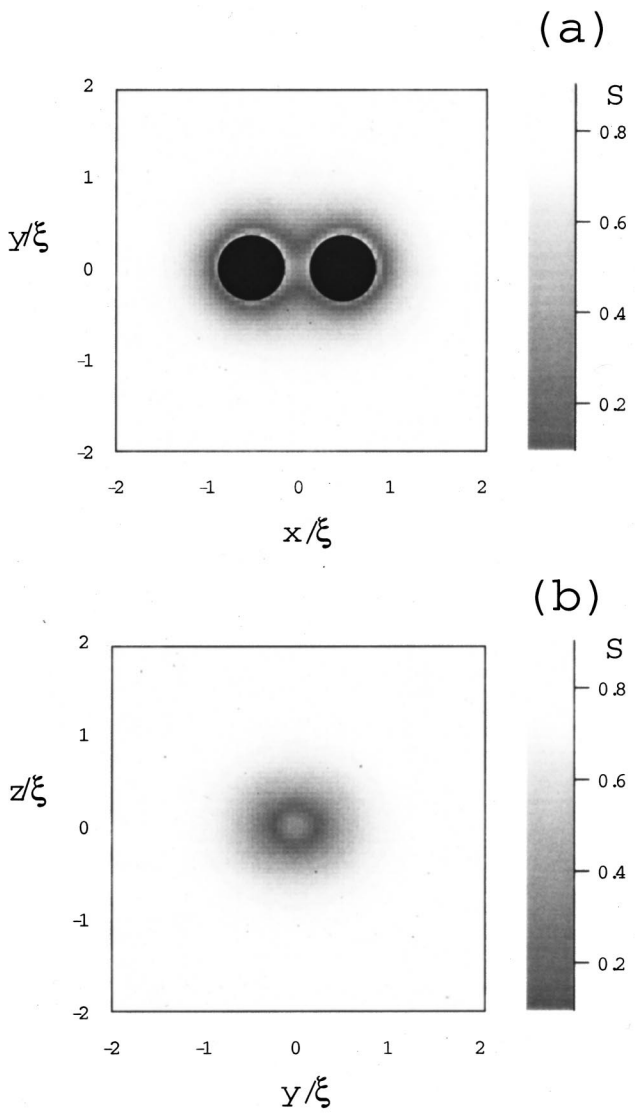

FIG. 12. Nematic scalar order parameter S for two particles in three dimensions: in the plane $x-y$ (a), in the midplane $y-z$ between the two particles (b).

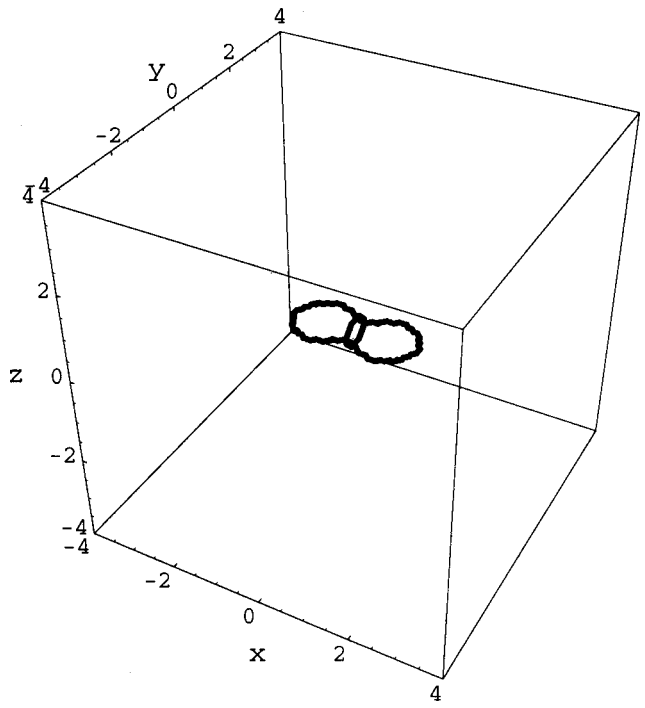

FIG. 13. Two particles in a nematic: three-dimensional visualization of the disclination lines. For particles at short distance, a circular disclination ring appears between the two colloidal particles.

tions in three dimensions, is particularly interesting. The corresponding nematic order parameter S is reported in Fig. 12 in the plane (x,y) and in the plane (y,z). The minimum in the order parameter, represented by the dark color, corresponds to the location of the disclination lines. The corresponding disclination lines are reported in Fig. 13. From these figures, one observes that the three-dimensional structure is characterized by the occurrence of a circular disclination line between the two particles. As the distance between the two particles increases, this circular ring becomes smaller. (This is similar to the two-dimensional calculations, where the defects in the midplane become closer to each other as the distance between the particles increases.) And, for sufficiently large separation distances, each particle is surrounded by its own Saturn ring without the presence of a circular ring between the particles.

Experimentally, different configurations have been observed for the binding of two colloidal particles at short distances. In the experiments of Poulin *et al.*,[27] one configuration corresponds to a linear chain of two particles, each of them being accompanied by a hedgehog defect. A different configuration has also been observed for which the particles are bound with a defect structure referred to as the "bubble-gum defect." As mentioned by the authors, the exact nature of this defect is unclear, although birefringent strings suggest that particles are connected by a disclination line. A correspondence between the bubble-gum defect and the defect structure presented in Fig. 13 cannot be established. The reason for that is that the bubble-gum defect has been observed when particles are aligned along the direction of the uniform nematic order[27] (particles aligned in the z direction), whereas the defect structure in Fig. 13 is obtained for particles perpendicular to the direction of nematic order. We have investigated the three-dimensional configuration when colloidal particles are aligned in the z direction. Our calculations reveal only configurations where particles are surrounded by their own Saturn ring, and they do not exhibit any defect structure that could explain the nature of the bubble-gum defect. (Investigations of other possible structures would require starting from initial ansatz configuration.) The defect structure presented in Fig. 13 is a new possible structure that, to the best of our knowledge, has not yet been observed experimentally.

V. CONCLUSION

The behavior of suspended particles in a uniform nematic liquid crystal has been studied with Monte Carlo simulations and dynamic field theory. A Monte Carlo method that combines a canonical expanded ensemble with a density of states formalism was implemented to evaluate potentials of mean force. A dynamic field theory was solved numerically to determine potentials of mean force and equilibrium configurations. Our results indicate good agreement with previous estimates for the location of defects in the limit of large particles, and show that deviations from the director description arise for small particles ($R \leqslant 8\sigma_0$ or $R \leqslant 4\xi$). Calculations on the interaction between a particle and a solid surface predict a global repulsive effective force, with the presence of local minima in the potential of mean force. These minima are due to layer formation near the wall. The structure of the nematic around two particles is also analyzed in two and three dimensions with the theory. Two-dimensional results indicate that particles with strong homeotropic anchoring at large distances are surrounded by their own Saturn ring defects and, for sufficiently short separation distances, the two defects interact with each other, leading to different director configurations and an effective attractive force. In three dimensions, a circular disclination line between the two particles is observed.

Comparison between molecular simulations and theory shows good quantitative agreement, and provides a good correspondence between the characteristic length introduced in the field theory with the length of the mesogens in the molecular description. This work also indicates that the theory, originally conceived to investigate the structure of a nematic at mesoscopic length scales, is also able to describe its structure down to molecular length scales.

ACKNOWLEDGMENT

This work is supported by the National Science Foundation through the University of Wisconsin's MRSEC on Nanostructured Interfaces.

[1] P. Poulin, H. Stark, J. C. Lubensky, and D. A. Weitz, Science **275**, 1770 (1997).
[2] V. K. Gupta, J. J. Skaife, T. B. Dubrovsky, and N. L. Abbott, Science **279**, 2077 (1998).
[3] V. K. Gupta and N. L. Abbott, Science **276**, 1533 (1997).
[4] N. Schophol and T. J. Sluckin, Phys. Rev. Lett. **59**, 2582 (1987).
[5] F. Brochard and P. G. de Gennes, J. Phys. (France) **31**, 691 (1970).

[6] E. M. Terentjev, Phys. Rev. E **51**, 1330 (1995).
[7] O. V. Kuksenok, R. W. Ruhwandl, S. V. Shiyanovskii, and E. M. Terentjev, Phys. Rev. E **54**, 5198 (1996).
[8] T. C. Lubensky, D. Pettey, N. Currier, and H. Stark, Phys. Rev. E **57**, 610 (1998).
[9] R. W. Ruhwandl and E. M. Terentjev, Phys. Rev. E **56**, 5561 (1997).
[10] H. Stark, Eur. Phys. J. B **10**, 311 (1999).
[11] S. Grollau, N. Abbott, and J. J. de Pablo, Phys. Rev. E **67**, 011702 (2003).
[12] J. L. Billeter and R. A. Pelcovits, Phys. Rev. E **62**, 711 (2000).
[13] D. Andrienko, G. Germano, and M. P. Allen, Phys. Rev. E **63**, 041701 (2001).
[14] E. B. Kim, R. Faller, Q. Yan, N. L. Abbott, and J. J. de Pablo, J. Chem. Phys. **117**, 7781 (2002).
[15] D. Chandler, *Introduction to Modern Statistical Mechanics* (Oxford University Press, New York, 1987).
[16] J. G. Gay and B. J. Berne, J. Chem. Phys. **74**, 3316 (1981).
[17] P. G. de Gennes and J. Prost, *The Physics of Liquid Crystals*, 2nd ed. (Clarendon, Oxford, 1993).
[18] M. Doi and S. F. Edwards, *The Theory of Polymer Dynamics* (Clarendon, Oxford, 1989).
[19] A. N. Beris and B. J. Edwards, *Thermodynamics of Flowing Systems* (Oxford University Press, Oxford, 1994).
[20] Simulations were performed with $A=1$, $L_1=0.55$, $D^*=0.35$. For a nematic potential $U=3$, these values imply $S^{eq}=0.5$, $\xi=1.81$, and $\Gamma=0.622$. Given suitable pressure, length, and time scales, these parameters can be mapped to $L_1=8.73pN$ and $\Gamma=6.22$ $Pa^{-1}\cdot s^{-1}$. The corresponding Frank elastic constants are then given by $K_{11}=K_{22}=K_{33}=4.37pN$. These material parameters values are representative of a $5CB$ liquid crystal.
[21] Two-dimensional simulations are performed with grids whose number of points varies from 324×324 to 500×500. We have used time steps varying in the range $0.000\,01\leqslant\Delta t\leqslant0.001$. Three-dimensional simulations are done with a grid $100\times100\times100$ and time steps varying in the range $0.0005\leqslant\Delta t\leqslant0.004$.
[22] S. Grollau, N. L. Abbott, and J. J. de Pablo, Phys. Rev. E **67**, 051703 (2003).
[23] J. Fukuda and H. Yokoyama, Eur. Phys. J. E **4**, 389 (2001).
[24] P. Poulin and D. A. Weitz, Phys. Rev. E **57**, 626 (1998).
[25] M. Tasinkevych, N. M. Silvestre, P. Patricio, and M. M. Telo de Gama, cond-mat/021004.
[26] R. W. Ruhwandl and E. M. Terentjev, Phys. Rev. E **55**, 2958 (1997).
[27] P. Poulin, V. Cabuil, and D. A. Weitz, Phys. Rev. Lett. **79**, 4862 (1997).